EMISSION SPECTRA OF WARM DENSE MATTER PLASMAS *

G. Miloshevsky[ξ], A. Hassanein
Center for Materials under Extreme Environment, School of Nuclear Engineering,
Purdue University, West Lafayette, IN 47907, USA

Abstract

Warm Dense Matter (WDM) is a highly transient state of material between cold condensed matter and dense plasmas. In this work, we have investigated the confinement of carbon ions in the WDM regime and the emission in spectral lines for WDM copper in a range of plasma temperatures and densities using the developed collisional-radiative equilibrium model that includes the effects of dense plasma on radiative properties. The 2s and 2p orbitals and charge density of carbon ions are found to be severely distorted at near-solid density. It is observed for WDM copper that with the increase of temperature, spectral lines disappear in infrared and visible spectrum regions and appear in ultraviolet and soft x-ray regions. At temperature >5 eV and low density (<0.1 g/cm^3), a significant amount of radiation is emitted in x-ray spectral lines. With the increase of mass density of WDM copper, the change in line shapes, their broadening and shifts are observed. At mass density of ~0.1 g/cm^3, the number of spectral lines is reduced, and completely disappear above solid density.

I. INTRODUCTION

Understanding the optical properties of rapidly expanding WDM plasmas is important to conducting experiments at the National Ignition Facility, since ignition targets may stay a relatively long time in this transient WDM regime [1]. The computation of radiative properties of WDM poses several challenges. The main influence of density effects on atoms and ions in a highly-coupled WDM plasma is lowering of their ionization potential, modification of energy levels, and broadening of spectral lines [2]. The accurate calculations of ionization balance, ion charge-state distributions, and atomic level populations of WDM plasmas are required.

We have developed and implemented the post-Hartree-Fock (HF) methods that include the effects of dense plasma environment on wavefunctions and electronic level structure of atoms and ions. The models involve the ion-sphere approximation with appropriate boundary conditions [3]. The radius of ion sphere, electron degeneracy, and collective effects of ions and electrons on the electronic structure of ions are calculated self-consistently. The outer-shell wavefunctions become strongly distorted and the energies of outermost atomic levels significantly increase. The valence electrons undergo delocalization. These atomic data are used in the collisional-radiative equilibrium (CRE) model [4] for calculations of radiative properties, opacities, photon transport, and radiative fluxes in WDM. The collisional cross-sections, ionization and recombination rates, and three-body collisions are corrected accounting for the dense plasma. A set of rate equations with coupling of ionic configurations, free electrons and photons is solved self-consistently within the CRE model. The results derived from these quantum models provide valuable insights into radiative properties of the WDM regime.

II. HARTREE-FOCK MODELS

The quantum models are developed to account for electron-electron correlations and degeneracy effects in the WDM regime. The Hartree-Fock-Slater (HFS) model [4] is recovered to the HF model. Due to the anti-symmetry of wavefunctions the potential of exchange interaction arises in the HFS and HF models. As a consequence, the electrons of the same spin avoid one another, a phenomenon called exchange or Fermi correlation. There is a space around an electron or the Fermi hole that excludes the electrons of the same spin. Thus, both the HFS and HF models account for the Fermi correlation: the energy of electron-electron interactions is reduced due to the reduction in probability of the same spin electrons approaching one another. However, the HFS model is an approximation to the HF model because the local Slater's exchange potential [5] is used instead of the non-local exchange HF potential. In the Slater's exchange potential, the *orbital-dependent* "exchange charge density" is replaced by the Fermi hole of a uniform electron gas (jellium). The HFS exchange potential doesn't exactly cancel self-interaction. Therefore, the HFS energy is higher than the HF energy. The HFS model [4] was recovered to the full HF model by replacing the HFS potential of exchange interaction by the HF potential of exchange interaction. The HF exchange potential cannot be expressed in terms of the usual charge density.

* Work supported by the Defense Threat Reduction Agency under Grant No. HDTRA1-11-1-0046
ξ email: gennady@purdue.edu

978-1-4799-2713-5/14/$31.00 ©2014 IEEE

It looks much like the Coulomb term, except that it switches or exchanges spin orbitals. The shape and structure of the HF exchange (Fermi) hole is different for various orbitals. It changes as a function of electron position. In the HF model, each electron is surrounded by an *orbital-dependent* exchange hole.

The experimental value of the ground state energy of Al is -242.752 a.u. (1 a.u. = 27.2 eV) [6]. The calculated HFS energy is -240.3 a.u. This energy is higher than the true energy by more than 60 eV. The HF energy of ground state is -241.9 a.u. that is still ~23 eV higher than the experimental value. It is observed that the ground energy is reduced about 20% for 2s, 2p and 3s HF orbitals of Al. The energy of outer 3p-orbital is reduced by ~30%. The comparison between HFS and HF orbitals and radial charge density of Al ground state demonstrates that accounting for a *non-local* HF exchange potential leads to small perturbations of 3p-orbital and insignificant variations of the charge density in the valence region (results are not shown).

The "mean field" description of the Coulomb interactions among electrons is used in the HFS/HF method. The wavefunction is approximated by a single Slater determinant. The effects due to the correlation of electron motions are not included. Single Slater determinant wavefunction cannot describe *nearly degenerate or degenerate states* (static correlation) and *rearrangement* of electrons (dynamic correlation) within partially filled subshells. In the "mean field" approximation, an electron interacts with an "averaged" charge density arising from the remaining electrons. However, the electrons undergo dynamic motions trying to avoid one another due to Coulomb repulsions at every instant of time. The inclusion of spatial correlations among electrons is necessary to accurately describe atomic properties.

To include the static and dynamic electron correlations, the Multi-Configuration Configuration-Interaction Hartree-Fock (MC/CI-HF) method is implemented. MC-HF corrects the most severe artifacts of the HF method by including *near-degenerate* states. The total wavefunction is approximated as a linear combination of *degenerate* Slater determinants with both coefficients and wavefunctions are minimized. In this way the proper arrangement of electrons around the nucleus is incorporated. The energy difference between MC-HF and HF is called the static correlation. In the CI-HF method, dynamic correlation is recovered by including Slater determinants describing *double, triple, etc. excitations*. Double, triple and quadruple excitations describe how many electrons move together or, in other words, the "correlation" between two electrons' motions, "three body correlations", and "four-electron correlations". In this way the electron motion with respect to each other and dependence on inter-electronic distance are incorporated. The mutual Coulomb repulsion between the electrons is reduced due to mixing of configurations with electrons occupying different orbitals (regions of space). The total CI-HF wavefunction is formed as a linear combination of such configurations where only expansion coefficients are variationally minimized. The energy difference between MC-HF and CI-HF is called the dynamical correlation. The dynamic and static correlation is, however, not well separable. The MC-HF also includes some dynamical correlation. Therefore, the MC-HF and CI-HF methods were implemented in a single code with a possibility to complement between the MC-HF and CI-HF calculations.

The combined MC/CI-HF method was used to calculate the wavefunctions, radial charge density, and energies of the ground state of atoms. A comparison of the HF and MC/CI-HF wavefunctions and radial charge density of Al is illustrated in Fig. 1. It can be seen that 1s and 2s orbitals treated as inactive are not changed. The inclusion of multiple configurations and configuration interactions perturbs the 2p, 3s and 3p orbitals (Fig. 1(a)). The radial distribution of charge density is affected in these orbitals (Fig. 1(b)). The second peak is reduced, and the well between peaks becomes deeper. The energy of outer 3s

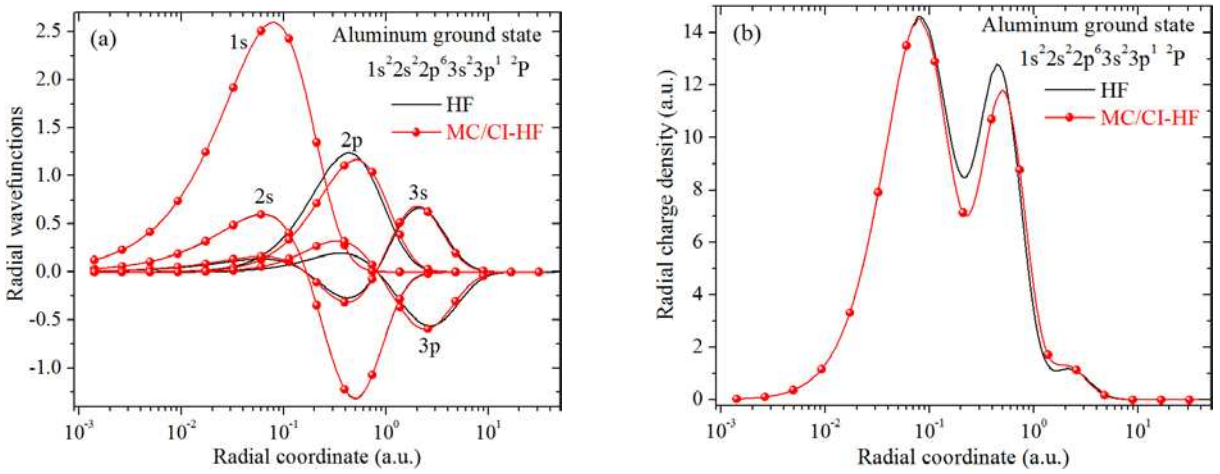

Figure 1. Comparison between radial HF and MC/CI-HF wavefunctions and charge density for aluminum ground state.

and 3p orbitals is found to be lower by ~10% and ~35%, respectively. The MC/CI-HF ground state energy of Al atom is -242.35 a.u. This is about ~12 eV lower compared to the HF energy. With account for relativistic correction energy, -0.4 a.u., the MC/CI-HF ground state energy -242.75 a.u. is very close to the experimental energy -242.752 a.u. [6].

III. EFFECTS OF DENSE ENVIRONMENT

In a dense plasma, the wavefunctions are affected by free electrons and neighboring ions. The MC/CI-HF methodology developed for isolated atoms is modified to include the effects of dense plasma environment. The structure of MC/CI-HF equations for a free atom are modified by including an additional radial potential into the Hamiltonian. The MC/CI-HF equations are then solved with modified boundary conditions on the outer boundary. Thus, the actual plasma environment for every ion is replaced by the boundary conditions for the electronic wave functions within a spherical volume centered at the nucleus. This is so-called an ion-sphere approximation [3]. The plasma is divided into neutral

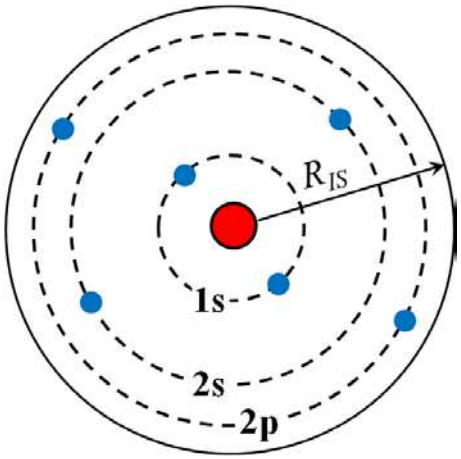

Figure 2. Carbon atom confined in a spherical cell with the ion sphere radius R_{IS} .

spherical cells. A sphere is constructed around each ion with the point charge Ze in such a way that the neutralizing electrons exactly cancel the charge of the ion (Fig. 2). Some of these electrons can be bound and some of them are free. The radius of ion sphere is given by

$$R_{IS} = \left(\frac{3A}{4\pi\rho N_A} \right)^{\frac{1}{3}}, \qquad (1)$$

where ρ is the mass density of plasma, N_A is Avogadro's number, and A is the atomic weight. With the decrease of a sphere radius (large mass density in Eq. (1)), the outer electrons can become delocalized. They are no longer bound to the atom, but are still confined within the sphere. The confinement potential that is added to the Hamiltonian to simulate the effect of dense environment is chosen to be of the form

$$U_c(r) = \left(\frac{r}{R_{IS}} \right)^m, \qquad (2)$$

where r is the radial coordinate and m is the degree of barrier stiffness. For $R_{IS} \to \infty$, the influence of $U_c(r)$ on wavefunctions is negligible and the solution is that of a free atom. For large m and small R_{IS}, this is a hard wall confinement potential. An infinitely high wall at the radius of the confining sphere corresponds to an impenetrable barrier. In this case, the radial wavefunctions are forced to zero at $r \geq R_{IS}$. By manipulating the value of m, the hardness of the confinement potential can be adjusted. This allows to account for a very small but finite penetration depth of the potential barrier. We have used $m = 25$ that produces a sufficiently stiff potential barrier. An infinitely high wall poses computational stability problems because several wavefunction nodes may not coincide with the radius of sphere for multi-electron atoms. The impenetrable barrier is not a good assumption, since the atom is effectively isolated from the rest of the system. A potential of finite depth should be used to model the realistic cases.

We have studied the radial wavefunctions, charge distribution, averaged orbital radii and energies, and the energy of the ground state of carbon atoms under the confinement by solving the MC/CI-HF problem. Carbon is open-shell atom ($1s^2 2s^2 2p^2$). The value of the mass density ρ was varied from 10^{-3} g/cm^3 to 10 g/cm^3. Depending upon ρ (Eq. (1)), the ion-sphere radius R_{IS} ranges from ~35 to ~1.5 a.u. The wavefunctions and charge density distribution as a function of radial coordinate are shown in Fig. 3. The curves are displayed for three densities 10^{-3} g/cm^3, 1.6 g/cm^3 and 10 g/cm^3 corresponding to the ion-sphere radii of 32 a.u., 2.7 a.u and 1.5 a.u. For the mass density of carbon plasma larger than 0.1 g/cm^3, it is found that the perturbation of wavefunctions and charge density occurs. For ρ = 1.6 g/cm^3, 2p and 2s orbitals are strongly perturbed (Fig. 3(a)). They approach zero on the ion sphere boundary at 2.7 a.u. The core 1s orbital is not influenced. The second peak of charge density is also highly perturbed (Fig. 3(b)). However, the first peak of charge density is not affected. Further increase in the charge density beyond the solid carbon density, ρ = 2.26 g/cm^3, leads to even higher distortion of 2s and 2p orbitals (Fig. 3(a)). For ρ = 10 g/cm^3, these orbitals are forced to zero at R_{IS} = 1.5 a.u. The 1s orbital remained still unperturbed. Both peaks of the charge density are strongly perturbed (Fig. 3(b)). Thus, we have observed that in the WDM plasma-like

state, wavefunctions and charge density of open-shell carbon are severely perturbed due to the density effects.

We have also investigated how the energies of occupied orbitals and the ground-state energy are varied during compression (results are not shown). The deep core 1s level is well separated from the outermost 2s and 2p levels. In the range of mass density from 10^{-3} g/cm^3 to ~0.1 g/cm^3, the orbital and total energies of carbon atom were not changed. The ground-state energy is -37.56 a.u. However, it was observed that the energy of all three orbitals and the total ground-state energy are strongly affected by large mass density. As the atom is compressed, the energy of the outermost 2p and 2s orbitals approaches zero and four electrons become delocalized within the ion sphere. The delocalization of 2p electrons was reached at R_{IS} ~2.7 a.u. (ρ ~1.6 g/cm^3). The delocalization of 2s electrons was achieved at R_{IS} ~2 a.u. (ρ ~3.6 g/cm^3). The energy of the 1s core orbital was increased by ~2 a.u. For ionization purposes, the perturbation of this deep level can be ignored. At the compression to R_{IS} ~2 a.u., the energy levels all shift by the same amount.

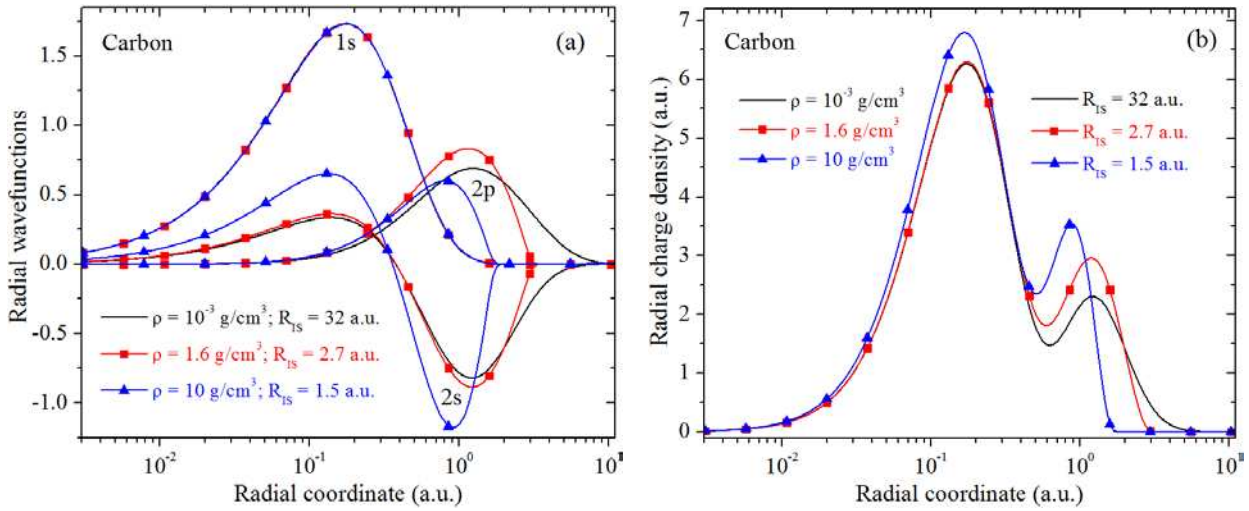

Figure 3. Radial wavefunctions (a) and electronic charge densities (b) as a function of radial coordinate for different mass densities of carbon.

IV. CRE MODEL FOR DENSE PLASMAS

The calculation of radiation properties of WDM poses several challenges. Density effects such as continuum lowering, collectivized electrons, and degeneracy effects become of significant importance in highly-coupled dense plasmas. The main influence of dense plasma environment on the ions is a lowering of their ionization potential, modification of the energy levels and broadening of the spectral lines due to pressure. The absorption and emission lines also undergo shifts relative to free atomic lines and changes of their shapes. The accurate calculations of ionization balance, ion charge-state distributions and atomic level populations are fundamental to the determination of radiative opacities. The interplay of numerous collisional and radiative processes modifies transition rates and ionization state.

The "distorted" MC/CI-HF wave functions were used to calculate "plasma density"-modified radiative transitions, cross sections of radiative emission, bremsstrahlung, ionization and recombination rates. These atomic data are implemented in the previously developed CRE model [4]. A set of rate equations with coupling of ionic configurations, free electrons and photons is solved self-consistently within the CRE model. The physics of bremsstrahlung emission and absorption, and electron-ion collisions is modified due to the strong ionic coupling effects. The collisional cross-sections, ionization and recombination rates, and three-body collisions are corrected. Specifically, the collisional ionization and 3-body recombination rates are changed. The semi-empirical Lotz formula for the ionization rate coefficient was corrected to account for the effect of ionization potential lowering. The correction factor is then determined and the ionization rate is multiplied by this factor to account for pressure ionization. Due to the detailed balance, the correction factor to the ionization rate was also used to correct the 3-body recombination rate. However, the relation between the ionization and recombination rates is also affected by the potential lowering. Therefore, the 3-body recombination rate is additionally multiplied by an exponential factor accounting for the reduction of ionization potential. The rates of radiative and di-electronic recombination are also affected. However, at high densities when the pressure ionization is important, the main recombination process is the 3-body recombination, and corrections to radiative and di-electronic recombination rates can be neglected. The processes of radiative excitation and radiative

ionization are taken into account in an approximation of the escape factor for spectral lines and direct radiative ionization for the continuum spectrum. This accounts for absorption and re-emission of photons in different parts of the plasma, thus facilitating energy transport and its redistribution. The Stark broadening of spectral lines in dense plasmas due to the micro-fields of nearby ions was also included. The line shape due to Stark broadening was expressed through the micro-field distribution function and Stark shifts caused by the micro-fields.

calculated from the Kirchhoff law as $\varepsilon_\nu = \kappa_\nu B_\nu$, where κ_ν is the absorption coefficient and B_ν is the Planck function. In the absence of LTE, the emissivity is always smaller than that determined from the Kirchhoff law. It is suitable to introduce the coefficient κ'_ν that shows the degree of deviation from κ_ν. The coefficient κ'_ν is calculated from the CRE model using the MC/CI-HF atomic data. We will call κ'_ν as the emission coefficient.

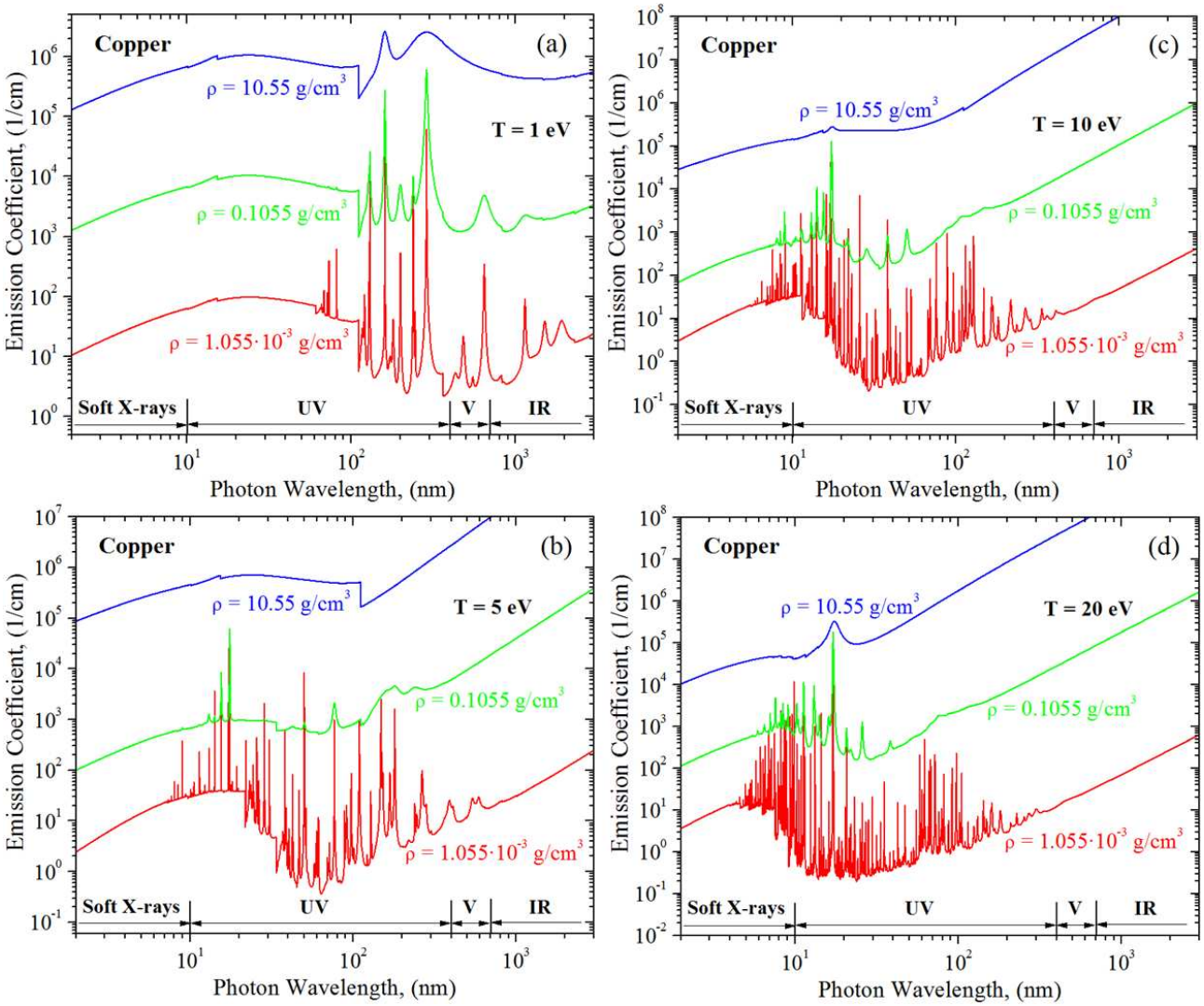

Figure 4. Emission coefficient of copper plasma as a function of photon wavelength for plasma temperatures of 1 eV (a), 5 eV (b), 10 eV (c) and 20 eV (d). In each panel, the emission is shown for three densities: $1.055 \cdot 10^{-3}$ g/cm^3, 0.1055 g/cm^3 and 10.55 g/cm^3.

V. PHOTON EMISSION FROM WARM DENSE COPPER

It is known that under local thermodynamic equilibrium (LTE) conditions the plasma emissivity ε_ν can be

It should be not confused with the emissivity that is also sometimes called the emission coefficient in the literature. The non-LTE emissivity can be then calculated as $\varepsilon_\nu = \kappa'_\nu B_\nu$.

The emission in spectral lines of copper plasma is shown in Fig. 4 for plasma temperatures 1, 5, 10, and 20 eV. In each panel, the emission coefficient as a function

of photon wavelength is illustrated for three densities: $1.055 \cdot 10^{-3}$, 0.1055 and 10.55 g/cm^3 that correspond to the number densities of 10^{19}, 10^{21} and 10^{23} cm^{-3}, respectively. The solid density of copper is 8.92 g/cm^3. The photon wavelength is divided into four regions corresponding to the soft x-rays, ultraviolet (UV), visible (V) and infrared (IR) portions of the spectrum. At T=1 eV and low density (10^{19} cm^{-3}), there is a number of spectral lines in the IR, V, and UV regions of spectrum (Fig. 4(a)). The spectral lines are already slightly broadened due to the density effects and represent a combination of overlapped individual spectral lines. In the IR region, the most intensive lines are located at 1148, 1511, and 1925 nm. In the V range, there are two lines at 482 and 646 nm. The largest number of strong spectral lines is located in the UV range. In the far (122 - 200 nm) and middle (200 - 300 nm) UV range, there are spectral lines at 128.8, 160.7, 199.6 nm (far UV) and 238.6 and 288 nm (middle UV), respectively. A separate group of spectral lines at 68.4, 73.4 and 81.6 nm is located in the extreme UV region. With increasing the mass density by two orders of magnitude (0.1055 g/cm^3), the spectral lines in the V and IR regions are further broaden and overlap forming two wide lines (Fig. 4(a)). The group of spectral lines in the extreme UV region doesn't survive. However, the lines in the far and middle UV range still remain, although the intensity of spectral lines at 128.8, 199.6 and 238.6 nm is decreased. The other lines at 160.7 and 288 nm remain quite intensive. Further increase of mass density to 10.55 g/cm^3 washes out the spectral lines in the IR and V ranges (Fig. 4(a)). The spectral lines at 160.7 and 288 nm are transformed to small and wide peaks. As the temperature of plasma increases to 5 eV (Fig. 4(b)), the spectral lines in the IR and V region disappear or their intensity is significantly reduced. Numerous new lines develop in the vacuum and extreme UV range. The most intensive spectral line is located at 17.5 nm. At T = 5 eV, the emission of photons in the spectral lines is already observed in the soft x-ray portion of the spectrum. The line with highest emission is located at 8.94 nm. The increase of mass density to 0.1055 g/cm^3 results in disappearance of spectral lines in the soft x-ray region. The majority of lines also disappear in the UV region. However, the most intensive line at 17.5 nm still remains. Further increase of mass density to 10.55 g/cm^3 leads to a complete washing-out of all lines in the spectrum. At higher plasma temperatures T = 10-20 eV (Figs. 4(c) and 4(d)), the line spectrum is shifted further toward the shorter wavelengths. A considerable amount of spectral lines appears in the soft x-ray region, especially at higher temperature (20 eV). The emission in spectral lines within both soft x-ray and UV ranges is still occurred at mass density of 0.1055 g/cm^3. For both T = 10 eV and T = 20 eV (Figs. 4(c) and 4(d)), the most intense line is located at 17.5 nm. No emission in spectral lines is seen at the mass density of 10.55 g/cm^3 that is slightly higher than the solid density of copper.

VI. SUMMARY

The HFS/HF models are recovered to MC/CI-HF models in order to include the static and dynamic electron-electron correlations. It is found that the MC/CI-HF quantum methods beyond mean-field theories significantly improve accuracy of atomic data accounting for near-degenerate and degenerate configurations and correlated electron-electron interactions.

The MC/CI-HF model is further upgraded to include the effects of plasma density on radial wavefunctions, charge density, atomic energy levels, averaged orbital radii, and ground-state energy. It is observed that under confinement, the 2s and 2p orbitals and charge density of carbon atoms are severely distorted. The electrons from both 2s and 2p orbitals are unbound and delocalized at $\rho \sim 3.6$ g/cm^3. For small confinement radii, the ground-state energy of carbon atoms increases sharply with density increase.

The CRE model for calculations of opacities and photon transport in WDM is upgraded to include the effects of dense plasma on radiative properties. The emission in spectral lines is investigated for WDM copper for a range of plasma temperatures and densities. With temperature increase, the spectral lines disappear in the infrared and visible regions and appear in the ultraviolet and soft x-ray regions. At temperature >5 eV and low density (<0.1 g/cm^3), a significant amount of radiation is emitted in the x-ray spectral lines. With the increase of mass density of copper plasma, the change in line shapes, their broadening, and shifts are observed. At mass density of ~0.1 g/cm^3, the number of spectral lines in the emission spectrum is significantly reduced, and they completely disappear above solid copper density.

VII. REFERENCES

[1] R. W. Lee, D. Kalantar, and J. Molitoris, “Warm Dense Matter: An Overview,” UCRL-TR-203844, Apr. 29 2004, Available: https://e-reports-ext.llnl.gov/pdf/307164.pdf

[2] G. Chiu and A. Ng, "Pressure ionization in dense plasmas," Phys. Rev. E, vol. 59, pp.1024-1032, Jan. 1999.

[3] J. C. Stewart and K. D. Pyatt, "Lowering of Ionization Potentials in Plasmas," Astrophys. J., vol. 144, pp. 1203-1211, Jun. 1966.

[4] S. S. Harilal, G. V. Miloshevsky, T. Sizyuk, and A. Hassanein, "Effects of excitation laser wavelength on Ly-α and He-α line emission from nitrogen plasmas," Phys. Plasmas, vol. 20, pp. 013105, Jan. 2013.

[5] J. C. Slater, "A Simplification of the Hartree-Fock Method," Phys. Rev., vol. 81., pp. 385-390, Feb. 1951.

[6] A. Veillard and E. Clementi, "Correlation Energy in Atomic Systems. V. Degeneracy Effects for the Second-Row Atoms," J. Chem. Phys., vol. 49, pp. 2415-2421, Sep. 1968.